Journal of Power Sources 263 (2014) 13–21

Contents lists available at ScienceDirect

Journal of Power Sources

journal homepage: www.elsevier.com/locate/jpowsour

A green method to prepare Pd–Ag nanoparticles supported on reduced graphene oxide and their electrochemical catalysis of methanol and ethanol oxidation

Lingzhi Li [a], Mingxi Chen [a], Guanbo Huang [a], Nian Yang [a], Li Zhang [a], Huan Wang [a], Yu Liu [a,c,*], Wei Wang [b], Jianping Gao [a,c,*]

[a] School of Science, Tianjin University, Tianjin 300072, PR China
[b] School of Chemical Engineering, Tianjin University, Tianjin 300072, PR China
[c] Collaborative Innovation Center of Chemical Science and Engineering, Tianjin 300072, PR China

HIGHLIGHTS

- The process without any dispersants, Ag–Pd bimetallic nanoparticles homogeneously distribute on the support.
- The reduction of Ag^{+}, K_4Pd^{2-} and GO depends on the reaction between $AgNO_3$, K_2PdCl_4 and GO instead of reductant.
- The samples have better catalytic property for alcohol electrocatalytic oxidation than many other Pd-based catalysts.

ARTICLE INFO

Article history:
Received 27 December 2013
Received in revised form
23 March 2014
Accepted 6 April 2014
Available online 15 April 2014

Keywords:
Bimetal
Graphene
Fuel cell
Catalyst

ABSTRACT

Bimetallic palladium–silver nanoparticles (NPs) supported on reduced oxide graphene (RGO) with different Pd/Ag ratios (Pd–Ag/RGO) were prepared by an easy green method which did not use any additional reducing agents or a dispersing agent. During the process, simultaneous redox reactions between $AgNO_3$, K_2PdCl_4 and graphene oxide (GO) led to bimetallic Pd–Ag NPs. The morphology and composition of the Pd–Ag/RGO were characterized by transmission electron microscopy, X-ray diffraction, X-ray photoelectron spectroscopy, thermogravimetric analysis and Raman spectroscopy. Cyclic voltammetry and chronoamperometry were used to investigate the electrochemical activities and stabilities of these Pd–Ag/RGO catalysts for the electro-oxidation of methanol and ethanol in alkaline media. Among the different Pd/Ag ratios, the Pd–Ag (1:1)/RGO had the best catalytic activities and stability. So it is a promising catalyst for direct alcohol fuel cell applications.

1. Introduction

In recent years, fuel cells have become a hot topic because of the decrease in fossil fuel reserves and the serious environmental pollution caused by the use of these fossil fuels. Fuel cells have shown great potential as highly efficient and low-emission power sources for portable electronic devices. Alcohols, like methanol and ethanol, are widely recognized as the most promising candidates for fuel cells [1–4]. Although fuel cells have been extensively studied, they still have many issues like a shortage of appropriate anodic catalysts and low catalytic activities [5]. The noble metal Pt is the most widely studied anodic catalyst in acidic media, but Pt-based catalysts have serious kinetic constraints because of poisoning by the reaction intermediates such as CO. This can gradually reduce the activity and stability of Pt-based catalysts. In addition, the high cost and limited availability of Pt does not allow it to be used at a commercial level which also severely limits the use of direct alcohol fuel cell technology [6–8]. It has been reported that Pt-based catalysts have better reaction kinetics in alkaline media and that some non-Pt based catalysts can also be used under alkaline conditions [9]. One catalyst that has received a great deal of attention is Pd because it has super catalytic activity and stability in direct alcohol fuel cells and it is about 50 times more abundant than Pt [10–13].

It has been proven that the catalytic activity and stability of nanoparticles (NPs) depend on their size and morphology [14,15]. However NPs easily aggregate which decreases their surface energy [16]. Therefore, suitable supports are needed to avoid aggregation. Vulcan XC-72R carbon black and carbon nanotubes are the most

* Corresponding authors. School of Science, Tianjin University, Tianjin 300072, PR China. Tel./fax: +86 2227403475.
E-mail address: jianpinggaols@126.com (J. Gao).

http://dx.doi.org/10.1016/j.jpowsour.2014.04.021
0378-7753/

common support materials for nanocatalysts [17] and the latter is better than the former [10,18]. However carbon nanotubes are so expensive that it limits their applications. Graphene is gradually becoming a popular new support material for NPs since it has many excellent properties some of which are better than those of other carbon materials. Its basal plane structure, large surface areas and high electrical conductivity all make graphene a good support material for nanocatalysts [19–21].

Since bimetallic NPs show better catalytic properties than monometallic NPs, they have been used to increase the catalytic activity of anodic catalysts [22]. Ag has been proposed to reduce the poisoning of CO-like species and increase the adsorption property, which increase the catalytic ability. It has been used as the second metal to Pt-based catalyst for methanol electrooxidation and obtains good performance [23]. So it's speculated the catalytic performance of Pd–Ag bimetallic NPs will be better than Pd NPs. Also Ag is abundant and fairly low price. It is inferred that Ag will be a good choice as a second metal.

Here, an easy method was developed to prepare reduced graphene oxide (RGO) supported Pd–Ag NPs (Pd–Ag/RGO), as shown in Fig. 1. Unlike previous methods, no additional reductants or surfactants were used. Instead, graphene oxide (GO) nanosheets acted as the reducing agent, the stabilizing agent and the support for the Pd–Ag NPs, so it is an environment-friendly method.

2. Experimental section

2.1. Materials

Natural graphite powder was purchased from Qingdao Graphite Factory. Potassium permanganate, sodium nitrate, concentrated sulfuric acid, hydrogen peroxide (30%), hydrochloric acid, potassium palladium (II) chloride (K_2PdCl_4) and silver nitrate were all from Sigma. All other reagents were purchased from Tianjin Chemical Reagent Co. All chemicals were analytical grade and used as received.

2.2. Preparation of GO

GO was prepared from purified natural graphite by a modified Hummer's method [24]. Briefly, concentrated H_2SO_4 was added to a 250-mL flask filled with graphite, followed by the addition of $NaNO_3$. Then solid $KMnO_4$ was gradually added with stirring while the temperature of the mixture was kept below 20 °C. Next the temperature was increased to 30 °C and excess distilled water was added to the mixture. Then the temperature was increased to 80 °C. Finally, 30% H_2O_2 was added until the color of mixture changed to brilliant yellow. The mixture was filtered and washed several times with 5% aqueous HCl to remove metal ions and then the product was washed with distilled water to remove the acid. The resulting filter cake was dried in air and then re-dispersed in water. Suspended GO sheets were obtained after ultrasonic treatment.

2.3. Synthesis of Pd–Ag/RGO

First 3 mL of $AgNO_3$ aqueous solution (0.0123 M) was mixed with 6.4 mL of GO suspension (5 mg mL^{-1}). Subsequently, about 0.5 mL of sodium hydroxide (0.05 M) was added to adjust the pH to 8.0. The mixture was heated at 84 °C and magnetically stirred for 0.5 h, followed by the addition of 3 mL of K_2PdCl_4 aqueous solution (0.0123 M). The mixture was allowed to continue to react under magnetic stirring at 84 °C for 3 h. Then the sample was cooled to room temperature. The reaction product was collected by centrifugation and washed several times with deionized water. Part of the purified product was thermally treated for 24 h at 200 °C in a vacuum oven to transform the GO to RGO, the other part of the product was used for measurements. The weight percent of Pd in the Pd–Ag/RGO was about 10 wt % and the atomic ratio of Pd to Ag was 1:1 (Pd–Ag (1:1)/RGO). In order to find which ratio led to the best catalytic activity, Pd–Ag (1.5:1)/RGO, and Pd–Ag (1:1.5)/RGO with the same 10 wt % of Pd were also prepared using the same procedure.

The most common method to synthesize RGO supported metal particles is chemical reduction. So for comparison, Pd–Ag NPs were also prepared using $NaBH_4$ instead of GO as the reducing agent. During this procedure the GO was also reduced by the $NaBH_4$. An excess amount of freshly prepared 0.01 M $NaBH_4$ was added to a mixed solution of K_2PdCl_4, $AgNO_3$ and GO to synthesize the Pd–Ag (1:1)/RGO–SB (that was reduced by $NaBH_4$).

2.4. Characterization

2.4.1. X-ray diffraction analysis

The X-ray diffraction (XRD) spectra of the samples were measured using an X-ray diffractometer (BDX3300) with a reference target: Cu Ka radiation (λ = 1.54 Å), voltage: 30 kV and current: 30 mA. The samples were measured from 30° to 90° (2θ) with steps of 4° min^{-1}.

2.4.2. Raman microscopy analysis

Raman measurement was performed with an inVia Raman Microscope (RENISHAW, UK) high resolution Raman microscope, in a backscattering configuration.

2.4.3. Thermogravimetric analysis

Prior to thermogravimetric analysis (TGA) of the samples, the samples were dried in a vacuum at 40 °C for 2 days. TGA was performed with a Rigaku-TD-TDA analyzer with a heating rate of 10 °C/min.

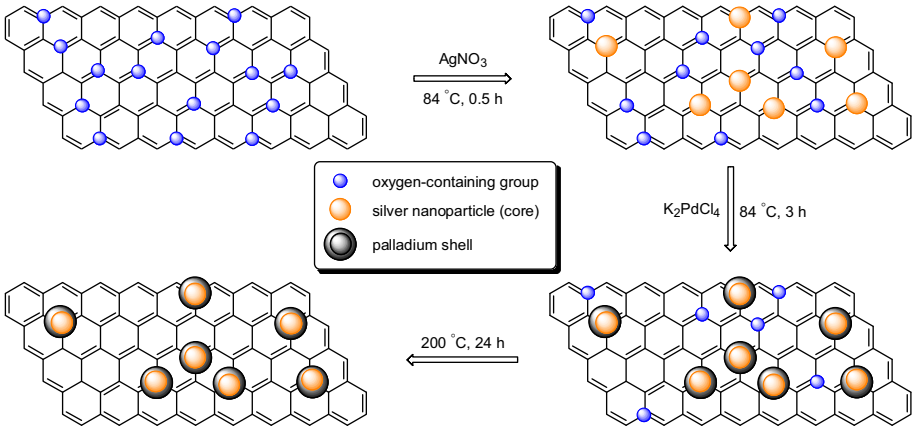

Fig. 1. Diagram of the synthesis of Pd–Ag NPs supported on RGO.

2.4.4. X-ray photoelectron spectroscopy (XPS) analysis

Elemental analysis was conducted on an X-ray photoelectron spectrometer with a Mg Kα anode (PHI1600 ESCA System, PERKIN ELMER, US).

2.4.5. Transmission electron microscopy (TEM) analysis

Transmission electron microscopy (TEM) and line profile measurements were performed using a Philips Tecnai G2F20 microscope at 200 kV.

2.4.6. Inductively coupled plasma (ICP) spectroscopy analysis

The amount of Ag and Pd elements on the solution after electrochemical measurements was determined by inductively coupled plasma spectroscopy (ICP-9000 (N + M), USA Thermo Jarrell-Ash Corp.).

2.5. Electrochemical measurements

The electrochemical measurements, cyclic voltammetry and chronoamperometry were performed with a CHI 660D electrochemical station (CH Instruments, Inc, Shanghai) at ambient temperature. The counter and reference electrodes were a platinum mesh and a Hg/HgO (1.0 M KOH) electrode, respectively. The working electrode was prepared by dropping 5 μL of the catalyst ink onto a glassy carbon electrode (GCE) with the diameter of 3 mm. The ink was prepared by ultrasonically mixing 4 mg of Pd–Ag/RGO

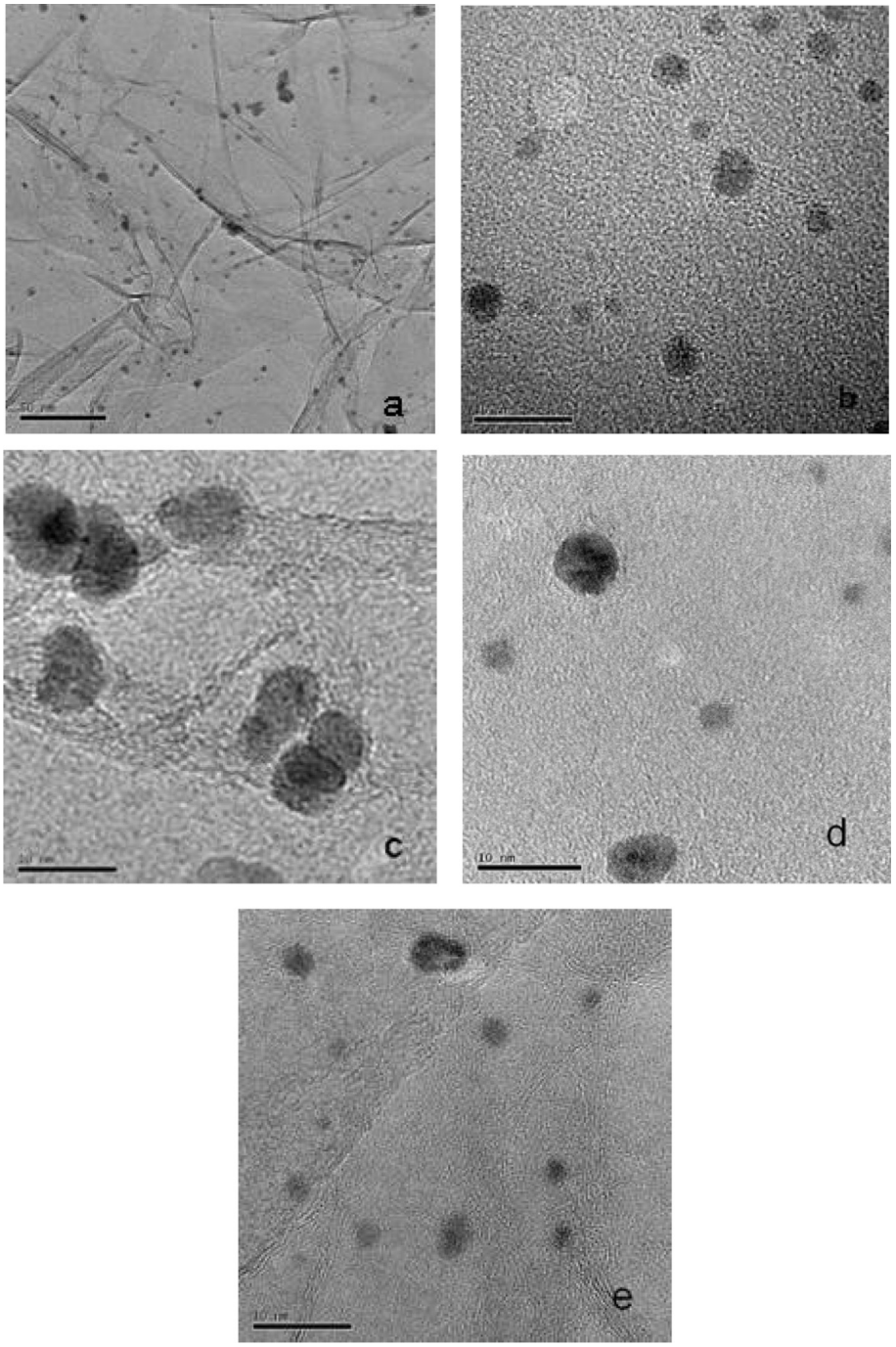

Fig. 2. TEM images of the Pd–Ag (1:1)/RGO (a and b), Pd–Ag (1.5:1)/RGO (c), Pd–Ag (1:1.5)/RGO (d), and Pd–Ag (1:1)/RGO–SB (e), magnified imagine of the Pd–Ag (1:1)/RGO (f).

with 1.9 mL of ethanol and 0.1 mL of Nafion solution. The electrolyte was 1 M KOH/1 M CH_3OH or 1 M KOH/1 M CH_3CH_2OH, and oxygen was removed by purging the electrolyte with an inert gas for 20 min.

3. Results and discussion

Fig. 2 shows the TEM images of the Pd–Ag/RGO NPs with different compositions. The corrugations of the graphene edges (Fig. 2a) are in accordance with a previous report for graphene [25]. The Pd–Ag (1:1) NPs are more uniform in size (Fig. 2b) than the Pd–Ag NPs for the other Pd/Ag ratios (Fig. 2c and d) or those reduced by $NaBH_4$ (Fig. 2e), and it's easy to see that most of the metallic NPs are smaller than 10 nm for all the samples. As we know, the alcohol electro-oxidation mechanism with metal catalyst is adsorption/desorption. So small size and good distribution are beneficial to the catalytic activity for direct alcohol fuel cell. In addition, RGO can increase electronic transmission speed and prevent aggregation of Pd–Ag in the electro-oxidation. Therefore, the Pd–Ag (1:1)/RGO should have good catalytic activity and stability for a direct alcohol fuel cell.

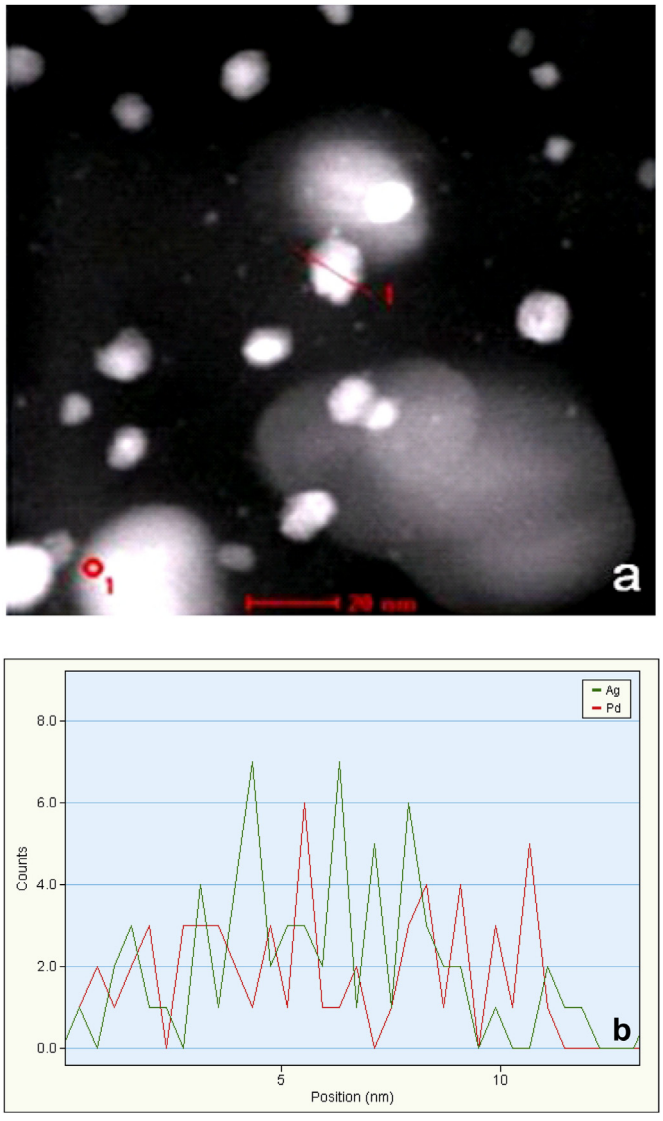

Fig. 3. The chosen particle (a), the line profile of the NP (b).

A metallic NP (Fig. 3a) was chosen for a line profile measurement (Fig. 3b). Obviously, both the Ag and Pd atoms are distributed over the whole area of the particle, but the core appears to be highly enriched with Ag atoms and the shell has more Pd atoms. In catalyzing some reactions Pd plays the key role, so the enriched Pd shell should result in an enhanced catalytic efficiency for electrochemical catalysis reactions [26].

Fig. 4 shows the XRD patterns of Pd/RGO (i) and Ag/RGO (ii) and three Pd–Ag/RGO NPs prepared with different ratios (iii–v). In the Pd/RGO diagram the peaks at about 40.1°, 46.3°, 68.5° and 81.8° corresponded to the (111), (200), (220) and (311) lattice planes of the face center cubic crystalline structure of Pd, respectively [18]. In the Ag/RGO diagram, the diffraction peaks at 38.0°, 44.2°, 64.5°, and 77.4° are assigned to the (111), (200), (220), and (311) crystalline planes of cubic Ag, respectively [27]. It's concluded that the XRD diagram of the three Pd–Ag/RGO samples is similar but none of the above peaks are seen (iii–v). All the peaks are located between the peaks of Pd and Ag, suggesting that Pd–Ag bimetal NPs were formed.

Fig. 5a shows the XPS spectrum of Pd–Ag (1:1)/RGO. There is a C_{1s} peak at about 284 eV, an O1s peak at about 530 eV, a Pd3d peak at about 340 eV and a Ag3d peak at about 372 eV which indicate that the Pd–Ag/RGO contains C, O, Pd and Ag respectively. The Pd and Ag are from metallic NPs whereas C and O are from RGO.

In order to study the changes in the GO, the high resolution C1s XPS spectra of GO, Pd–Ag (1:1)/GO and Pd–Ag (1:1)/RGO were collected and are shown in Fig. 5b–d. The percentages of different carbon–oxygen groups and the C/O ratio for these samples are given in Table 1. The XPS C1s spectra have peaks at 284.4, 286.3, and 288.6 eV which can be attributed to C=C double bonds, C–O single bonds, and C=O double bonds, respectively [28]. The relative intensity of the C–O and C=O peaks in Pd–Ag (1:1)/GO is smaller than those in GO and the C=C/C–O ratio increases from 1.22 to 2.84 (Table 1). This states that the oxygen-containing functional groups were partly removed in the reaction, which leaved defects on the surface of the GO. These defects provided binding sites for Pd–Ag NPs [29]. So oxygen-containing functional groups played an important role in the formation of the Pd–Ag/RGO. Thermal treatment can further reduce GO to RGO, so the C/O ratio in Pd–Ag (1:1)/RGO increased to 5.1, as the GO was 2.3 and Pd–Ag (1:1)/GO was 4.5.

Pd3d and Ag3d XPS spectra of Pd–Ag (1:1)/RGO were collected in order to study the valence states of the metals (Fig. 5e and f). The

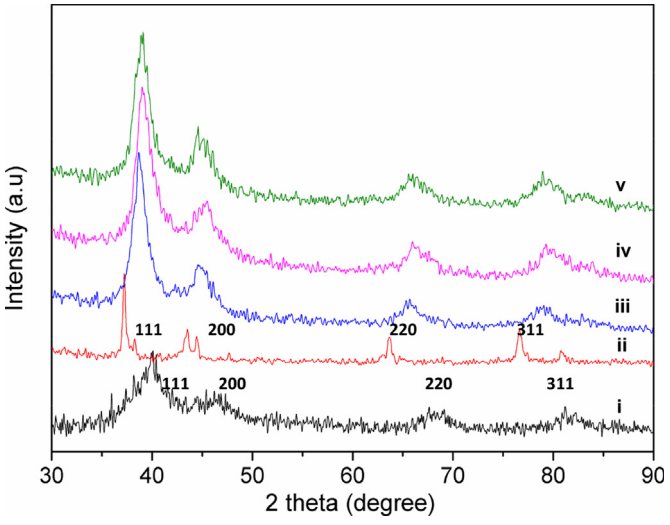

Fig. 4. XRD patterns of Pd/RGO (i), Ag/RGO (ii), Pd–Ag (1:1.5)/RGO (iii), Pd–Ag (1:1)/RGO (iv), and Pd–Ag (1.5:1)/RGO (v).

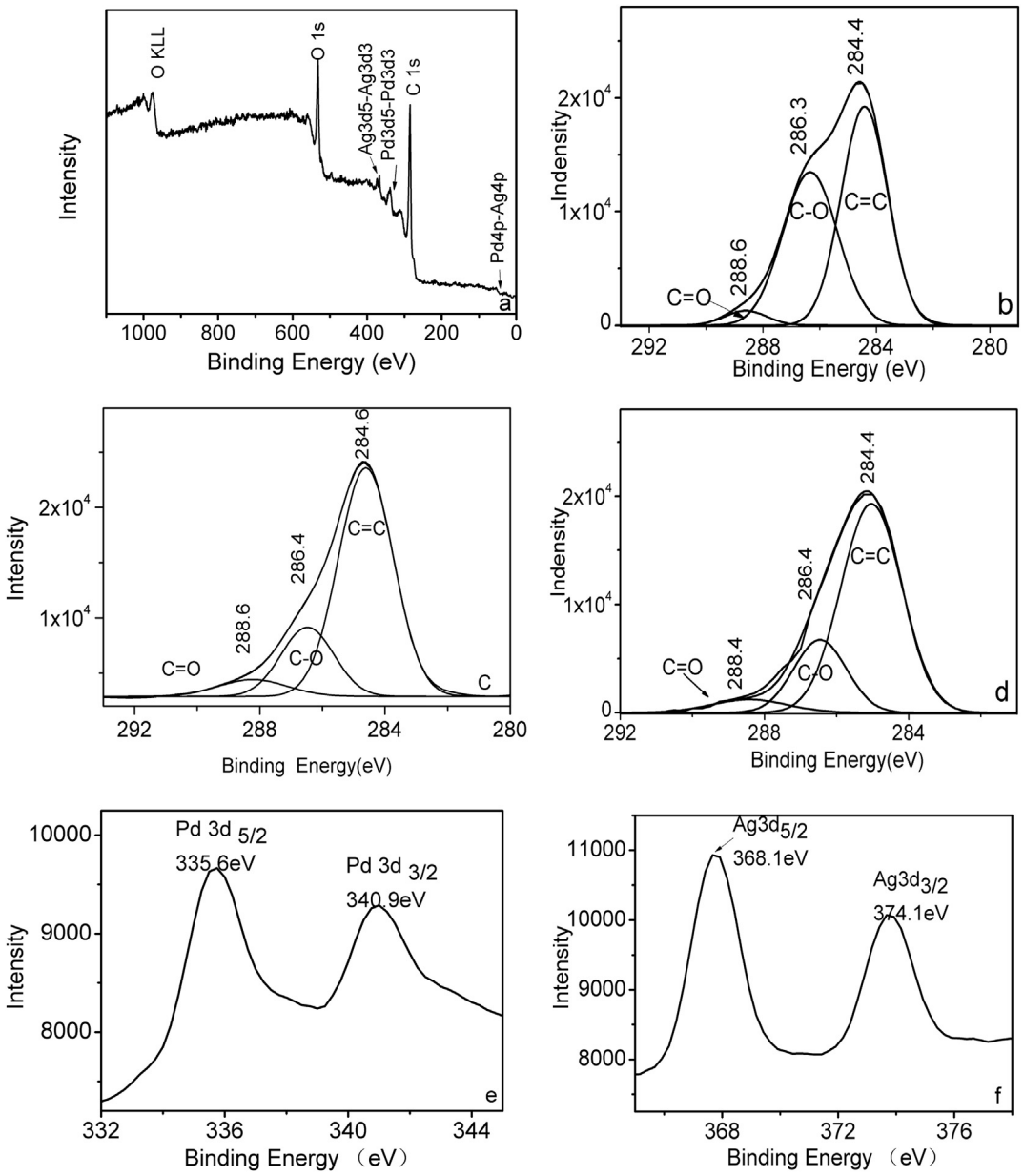

Fig. 5. XPS spectra for Pd–Ag (1:1)/RGO (a); C1s XPS spectra for GO (b), Pd–Ag (1:1)/GO (c) and Pd–Ag (1:1)/RGO (d); XPS spectra for Pd3d (e) and Ag3d (f) in Pd–Ag (1:1)/RGO.

Pd 3d5/2 peak at 335.6 eV and the 3d3/2 peak at 340.95 eV (Fig. 5e) are attributed to metallic Pd [30], and the peaks at 368.1 and 374.1 eV (Fig. 5f) can be ascribed to 3d5/2 and 3d3/2 of Ag, respectively [31]. Therefore, the $PdCl_4^{2-}$ and Ag^+ precursors were reduced during the reaction. The difference in the reduction potentials of $PdCl_4^{2-}$ (+0.83 V vs. SCE) and Ag^+ (+0.80 V vs. SCE) and the oxidation potential of GO (0.48 V vs. SCE) may be the driving force for the reduction of $PdCl_4^{2-}$ and Ag^+. It is rational to deduce that the spontaneous deposition of Pd–Ag NPs on GO is due to redox reactions between GO, Ag^+ and $PdCl_4^{2-}$, which is similar to the reaction mechanism between Pt precursor and single-walled carbon nanotubes proposed by Choi et al. [32].

The TGA curves of GO (i), Pd–Ag/GO (ii), and Pd–Ag/RGO (iii) are shown in Fig. 6. For GO, a weight loss of about 15% occurred between 100 and 200 °C which is attributed to the removal of water and some oxygen-containing functional groups (such as C–O and C=O). The weight loss above 200 °C is due to the removal of the other oxygen-containing functional groups. The weight loss in Pd–Ag/GO (ii) is smaller than that in GO and is only about 6% below 350 °C. This is in accordance with the XPS results which prove that the GO in Pd–Ag/GO was partially reduced. The total weight loss of Pd–Ag/RGO (iii) is much smaller than that of Pd–Ag/GO which indicates that the GO was greatly reduced after the thermal treatment.

Table 1
Percentages of different carbon–oxygen groups and C/O ratios in GO, Pd–Ag (1:1)/GO and Pd–Ag (1:1)/RGO.

Sample	Analysis			
GO	C=C	C–O	C=O	C/O ratio
	52.07	42.69	5.24	2.3
Pd–Ag (1:1)/GO	C=C	C–O	C=O	C/O ratio
	70.4	24.8	5.0	4.5
Pd–Ag (1:1)/RGO	C=C	C–O	C=O	C/O ratio
	78.4	16.8	4.8	5.1

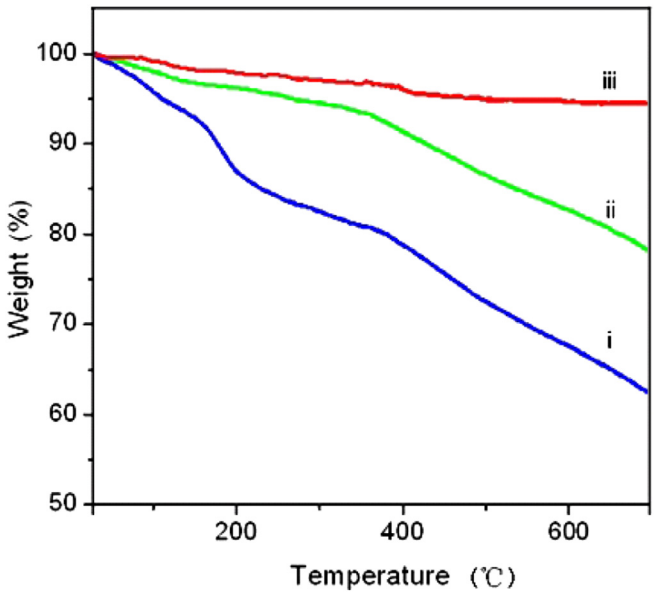

Fig. 6. TGA curves of GO (i), Pd–Ag/GO (ii), and Pd–Ag/RGO (iii).

Fig. 7 shows the Raman spectra of GO, Pd–Ag/GO and Pd–Ag/RGO. The two peaks at about 1355 and 1395 cm^{-1} are the D- and G-bands respectively [33]. The D-band is related to the vibrations of the sp^3 carbon atoms in the disordered graphene nanosheets, whereas the G-band arises from the vibrations of the graphite sp^2 carbon atom domains. The D/G intensity ratio is an indicator of the degree of in-plane sp^2 domains and the degree of GO reduction [27]. The D/G intensity ratio of GO (Fig. 7a) was 0.81 compared to 1.12 for Pd–Ag/RGO (Fig. 7c), which confirms that the oxygenated groups were removed during the thermal treatment process. The D/G intensity ratio of Pd–Ag/GO (1.03) is higher than that of GO, but lower than that of Pd–Ag/RGO, which again confirms that the GO in Pd–Ag/GO was partially reduced.

Next, the catalytic activity of the various Pd samples for the electro-oxidation of methanol and ethanol was tested. First the background cyclic voltammograms of Pd/RGO (i), Pd–Ag (1.5:1)/RGO (ii), Pd–Ag (1:1)/RGO (iii), Pd–Ag (1:1.5)/RGO (iv), Pd–Ag (1:1)/GO (v) and Pd–Ag (1:1)/RGO–SB (vi) modified electrodes in 1 M KOH at a scan rate of 50 mV s^{-1} between −0.8 and 0.3 V were collected (Fig. 8a). For all the catalysts, the adsorption/desorption of hydrogen appeared between −0.8 and −0.6 V, and the oxidation of Pd and the reduction peak for palladium oxide was around 0.4 V and −0.3 V respectively [18]. As there are no peaks of Ag and its oxide, it's inferred that Ag was stable in this system. The potential of Ag electrode is −0.0977 to 0.3023 V, and the pH is 14 during the methanol oxidation. According to the Pourbaix diagram (Fig. S1), Ag in Pd–Ag is almost in the stable region. In addition, the ICP results showed that there were no Ag and Pd elements in the solution of 1 M KOH and 1 M KOH/1 M CH_3OH after the electrochemical measurement. So, Ag in Pd–Ag NPs is stable and nonsoluble during electrochemical measurement. That is why Ag based bimetallic NPs were largely used in electrochemistry catalyst reaction [10,27].

The cyclic voltammograms of Pd/RGO (i), Pd–Ag (1.5:1)/RGO (ii), Pd–Ag (1:1)/RGO (iii), Pd–Ag (1:1.5)/RGO (iv), Pd–Ag (1:1)/GO (v) and Pd–Ag (1:1)/RGO–SB (vi) modified electrodes in 1 M KOH/1 M CH_3OH at a scan rate of 50 mV s^{-1} are shown in Fig. 8b. All the results are normalized on the basis of the amount of loaded Pd (mass activity). The oxidation peaks in the forward (I_f) and reverse (I_b) scans are due to the oxidation of freshly chemisorbed methanol species and to the removal of carbonaceous species that are not completely oxidized on the forward scan, respectively. The peak potentials, peak current densities and the ratio of I_f and I_b (I_f/I_b) are listed in Table 2. The Pd–Ag (1:1)/RGO reached 630 mA mg^{-1} Pd which was the highest of all the catalysts. The current density of Pd–Ag (1:1)/RGO is also higher than those of previously reported Pd–based catalysts, such as Pd/PPy–graphene (359.8 mA mg^{-1} Pd) [34], Pd–MnO_2/MWCNTs (431.02 mA mg^{-1} Pd) [35]. Moreover, when the ratio of Pd/Ag was 1:1, the peak potential was the most negative, indicating that the methanol was more easily oxidized. So among the studied Pd–Ag/RGO catalysts, Pd–Ag (1:1)/RGO has the highest catalytic activity.

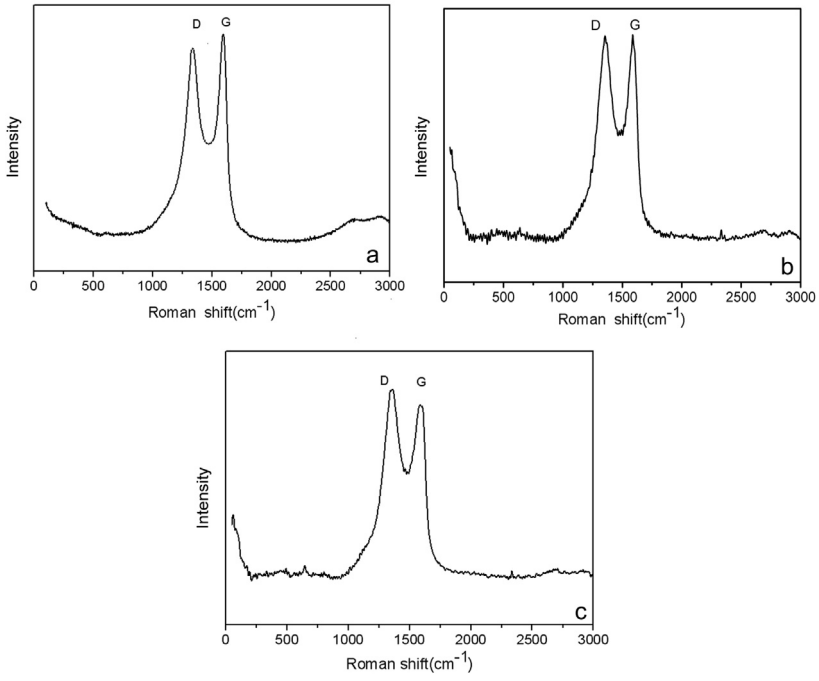

Fig. 7. Raman spectra of GO (a), Pd–Ag/GO (b), and Pd–Ag/RGO (c).

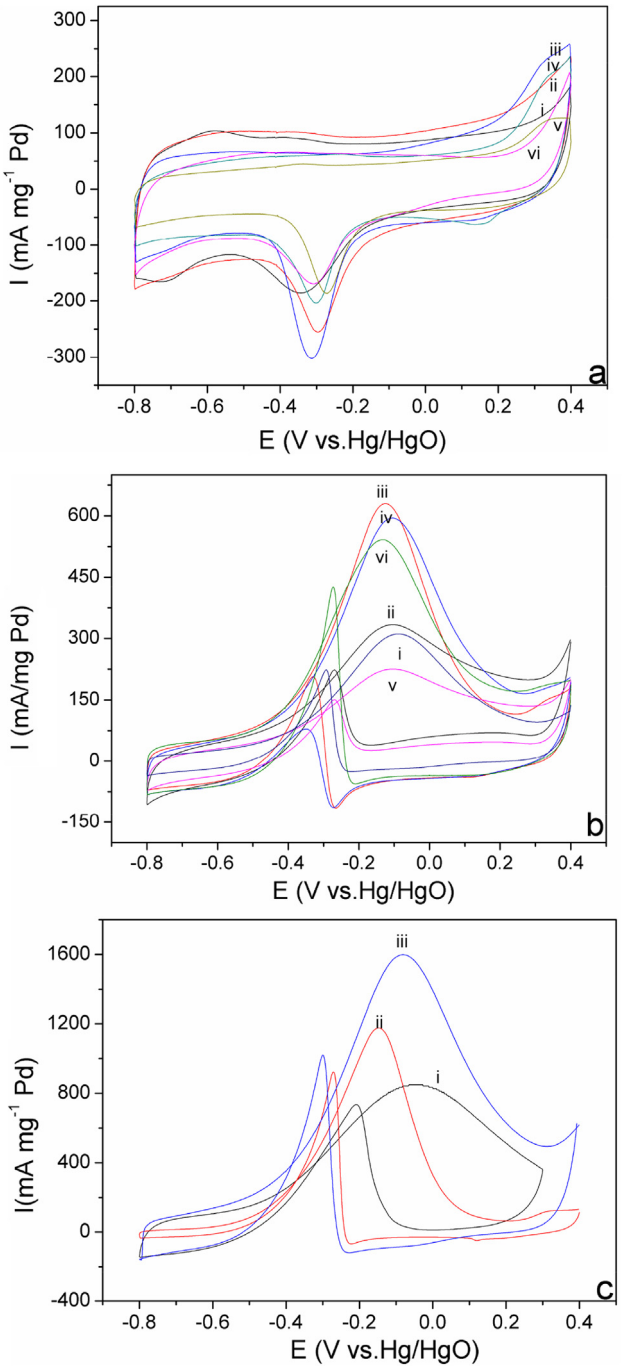

Fig. 8. Cyclic voltammograms of Pd/RGO (i), Pd–Ag (1.5:1)/RGO (ii), Pd–Ag (1:1)/RGO (iii), Pd–Ag (1:1.5)/RGO (iv), Pd–Ag (1:1)/GO (v), and Pd–Ag (1:1)/RGO–SB (vi) modified electrodes in 1 M KOH (a) and 1 M KOH/1 M CH_3OH (b) with a scan rate of 50 mV s^{-1}. Cyclic voltammograms of Pd/RGO (i), Pd–Ag (1:1)/RGO (ii), and Pd–Ag (1:1)/RGO–SB (iii) modified electrodes in 1 M KOH/1 M CH_2CH_3OH (c) with a scan rate of 50 mV s^{-1}.

The peak current density of Pd–Ag/RGO is much higher than that of the Pd/RGO (311 mA mg^{-1} Pd). The exact reason is not clear, but it may be attributed to the second metal Ag. It is proposed that Ag can provide synergistic effect in alcohol electrooxidation. It can provide oxygen-containing species to enhance the oxidation of CO-like species and reduce the poison of those species [23]. At the same time the second metal can modify the surface adsorption to increase the active surface of the major metal, which is an important factor to improve the catalytic activity and stability [36]. Another

Table 2
Peak potential, peak current density and I_f/I_b for various Pd-catalyst electrodes for the electro-oxidation of methanol.

Catalyst	Peak potential *V* vs. Hg/HgO	Peak current density mA mg^{-1} Pd	I_f/I_b
Pd/RGO	−0.08	311	1.41
Pd–Ag (1:1)/GO	−0.13	225	1.50
Pd–Ag (1.5:1)/RGO	−0.08	334	1.42
Pd–Ag (1:1)/RGO	−0.12	630	3.15
Pd–Ag (1:1.5)/RGO	−0.10	585	6.55
Pd–Ag (1:1)/RGO–SB	−0.125	545	1.48

key factor is the support, RGO. As shown in Table 2, the peak current density of Pd–Ag (1:1)/GO was 225 mA mg^{-1} Pd, which was much lower than that of Pd–Ag (1:1)/RGO. It was reported that the peak current densities for Pd NPs were 210 mA mg^{-1} Pd [37], 240 mA mg^{-1} Pd for Pd/C [11]. The above data prove that RGO is a better support than GO and other carbon materials. RGO has many advantages as a support. First, RGO has large surface areas, which makes the metal NPs smaller and more stable. Second, electrons transfer more quickly due to the high electrical conductivity of RGO.

The I_f/I_b ratio is an important index that reflects the tolerance of a catalyst to poisoning. A high I_f/I_b value indicates good oxidation of methanol to carbon dioxide during the forward scan and an excellent ability to remove any excessive accumulations of carbonaceous residue on the catalyst surface during the reverse scan [38,39]. As seen from Table 2, the Pd/RGO catalyst had the lowest I_f/I_b value among the catalysts. As the Ag content increased, the anti-poisoning effect was enhanced as seen by the high I_f/I_b values for Pd–Ag (1:1)/RGO (3.15) and Pd–Ag (1:1.5)/RGO (6.55). This trend is in accordance with a previous reported [23]. Since Pd–Ag (1:1)/RGO has both high catalytic activity and a high tolerance to poisoning species, the subsequent studies used this catalyst.

The catalytic activities of Pd/RGO, Pd–Ag (1:1)/RGO and Pd–Ag (1:1)/RGO–SB for the electro-oxidation of ethanol were also examined (Fig. 8c). The peak potentials, peak current densities and I_f/I_b values of these electrodes are listed in Table 3. For the electro-oxidation of ethanol, the Pd–Ag (1:1)/RGO still had the highest peak current density (1601 mA mg^{-1} Pd) indicating that Pd–Ag (1:1)/RGO is an excellent catalyst for alcohol electro-oxidation.

Fig. 9a shows the cyclic voltammograms of the Pd–Ag (1:1)/RGO modified electrode in 1 M KOH/1.0 M CH_3OH solution at different scan rates. Obviously, the peak current densities increased with increasing scan rate. The electrocatalytic oxidation of methanol is generally considered to be an irreversible electrode process and the peak current densities are linearly proportional to the square root of the scan rates [40]. As shown in Fig. 9b, the relationship between the forward scan peak current densities and $v^{1/2}$ is linear which is in accordance with the above dynamic theory. This also indicates that the electrocatalytic oxidation of methanol on Pd–Ag/RGO may be a diffusion controlled process.

The long-term stability of the Pd/RGO, Pd–Ag (1:1)/RGO and Pd–Ag (1:1)/RGO–SB catalysts for the oxidation of methanol and ethanol at a potential of −0.3 V were also investigated and the chronoamperometry curves are shown in Fig. 10. Due to the

Table 3
Peak potential, peak current density and I_f/I_b for various Pd electrodes for the electro-oxidation of ethanol.

Catalyst	Peak potential *V* vs. Hg/HgO	Peak current density mA mg^{-1} Pd	I_f/I_b
Pd	0.059	835	1.15
Pd–Ag (1:1)/RGO	0.082	1601	1.56
Pd–Ag (1:1)/RGO–SB	0.11	1170	1.27

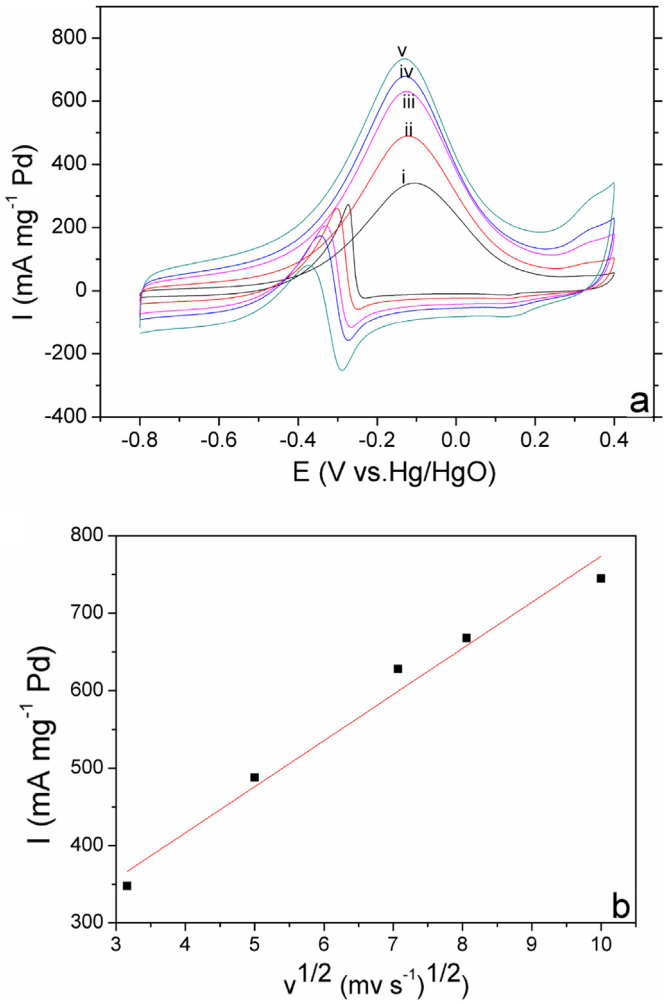

Fig. 9. Cyclic voltammograms of the Pd–Ag (1:1)/RGO-catalyst modified electrode in 1 M KOH/1 M CH_3OH at different scan rates 10 mV s^{-1} (i), 25 mV s^{-1} (ii), 50 mV s^{-1} (iii), 65 mV s^{-1} (iv) and 100 mV s^{-1} (v) (a). Plot of peak current densities versus the square root of the sweep rates (b).

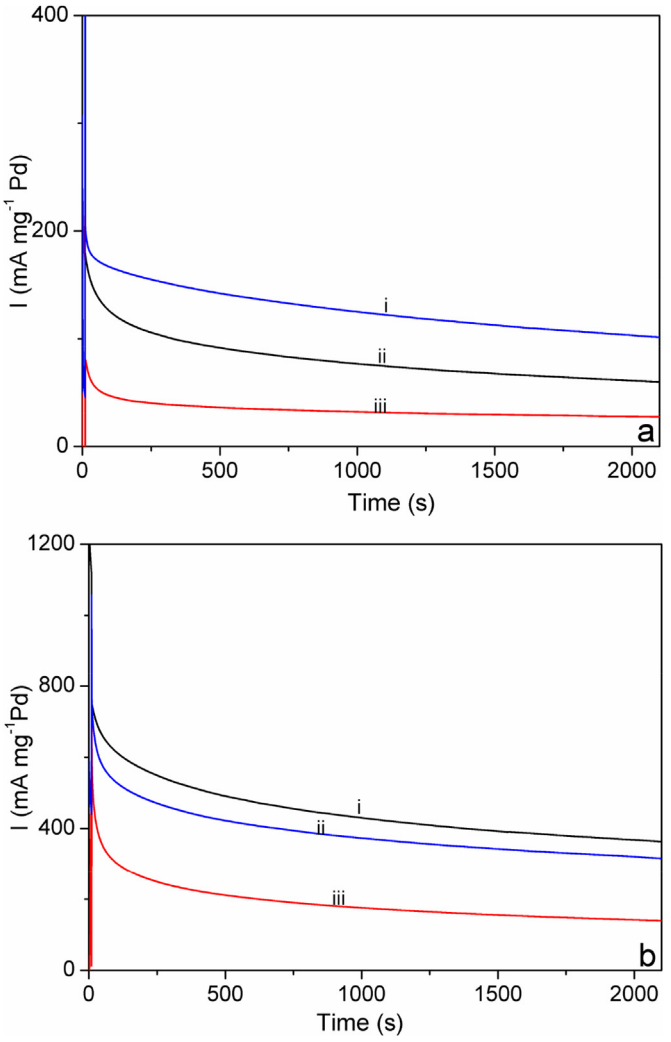

Fig. 10. Chronoamperometry curves collected for 2100 s at −0.3 V for Pd–Ag (1:1)/RGO (i), Pd–Ag (1:1)/RGO–SB (ii) and Pd/RGO (iii) modified electrodes in 1 M KOH/1 M CH_3OH solution (a), and 1 M KOH/1 M CH_3CH_2OH solution (b).

formation of some Pd oxides/hydroxides and adsorbed intermediates in the alcohol electro-oxidation reaction, all these catalysts show a current decay before a steady current status was attained. As expected, the current density of Pd–Ag (1:1)/RGO was the highest among the three catalysts in both alcohols. In addition, in the beginning, the current for Pd–Ag (1:1)/RGO declined more slowly than that for Pd/RGO and Pd–Ag (1:1)/RGO–SB. This also proves that Pd–Ag (1:1)/RGO has superior electrochemical catalytic stability for the oxidation of alcohols.

4. Conclusions

Pd–Ag/RGO hybrids with different Pd/Ag ratios were prepared by an easy green method without using any addition reducing agent or dispersing agent. Simultaneous redox reactions between $AgNO_3$, K_2PdCl_4 and GO led to bimetallic Pd–Ag NPs supported on RGO. The Pd–Ag/RGO hybrids exhibited good electrochemical catalytic activity towards methanol and ethanol electro-oxidation and Pd–Ag (1:1)/RGO had the best catalytic activity with peak current densities of 630 and 1601 mA mg^{-1} Pd for methanol and ethanol electro-oxidation, respectively. In addition, the Pd–Ag (1:1)/RGO showed high catalytic stability. This green method provides a way to produce Pd–Ag/RGO hybrids that can be used as electrochemical or chemical catalysts.

Acknowledgments

Funding from the National Natural Science Foundation of China, China (21202115, 21276181, and 21074089) is gratefully acknowledged.

Appendix A. Supplementary data

Supplementary data related to this article can be found at http://dx.doi.org/10.1016/j.jpowsour.2014.04.021.

References

[1] L. Wang, Y. Nemoto, Y. Yamauchi, J. Am. Chem. Soc. 133 (2011) 9674.
[2] R. Ganesan, J.S. Lee, Angew. Chem. Int. Ed. 44 (2005) 6557.
[3] Q.F. Yi, F.J. Niu, L.H. Song, X.P. Liu, H.D. Nie, Electroanalysis 23 (2011) 2232.
[4] C. Bianchini, P.K. Shen, Chem. Rev. 109 (2009) 4183.
[5] X. Zhao, M. Yin, L. Ma, L. Liang, C. Liu, J. Liao, Energy Environ. Sci. 4 (2011) 2736.
[6] F. Bensebaa, A.A. Farah, D.S. Wang, C. Bock, X.M. Du, J. Kung, Y.L. Page, J. Phys. Chem. B 109 (2005) 15339.
[7] Z. Liu, X. Zhang, L. Hong, Electrochem. Commun. 11 (2009) 925.
[8] R.M. Abdel Hameed, K.M. El-Khatib, Int. J. Hydrogen Energy 35 (2010) 2517.
[9] S.S. Gupta, J. Datta, J. Power Sources 145 (2005) 124.
[10] Y. Wang, Z.M. Sheng, H. Yang, S.P. Jiang, C.M. Li, Int. J. Hydrogen Energy 35 (2010) 10087.

[11] C.W. Xu, L.Q. Cheng, P.K. Shen, Y.L. Liu, Electrochem. Commun. 9 (2007) 997.
[12] Y.H. Qin, H.H. Yang, X.S. Zhang, P. Li, C.A. Ma, Int. J. Hydrogen Energy 35 (2010) 7667.
[13] R.N. Singh, A. Singh, Anindita, Carbon 47 (2009) 271.
[14] H. Lee, S.E. Habas, G.A. Somorjai, P.D. Yang, J. Am. Chem. Soc. 130 (2008) 5406.
[15] M.L. Pang, J.Y. Hu, H.C. Zeng, J. Am. Chem. Soc. 132 (2010) 10771.
[16] R.J. White, R. Luque, V.L. Budarin, J.H. Clark, D.J. MacQuarrie, Chem. Soc. Rev. 38 (2009) 481.
[17] L. Li, Y. Xing, J. Electrochem Soc. 153 (2006) A1823.
[18] F.H. Li, Y.Q. Guo, R.Q. Li, F. Wu, Y. Liu, X.Y. Sun, C.B. Li, W. Wang, J.P. Gao, J. Mater. Chem. A 1 (2013) 6579.
[19] J.S. Bunch, A.M. Van Der Zande, S.S. Verbridge, I.W. Frank, D.M. Tanenbaum, J.M. Parpia, H.G. Craighead, P.L. McEuen, Science 315 (2007) 490.
[20] S. Park, R.S. Ruoff, Nat. Nanotechnol. 4 (2009) 217.
[21] Y. Sun, Q. Wu, G. Shi, Energy Environ. Sci. 4 (2011) 1113.
[22] S.J. Guo, S.J. Dong, E. Wang, ACS Nano 4 (2010) 547.
[23] L.L. Feng, G. Gao, P. Huang, X.S. Wang, C.L. Zhang, J.L. Zhang, S.W. Guo, D.X. Cui, Nanoscale Res. Lett. 6 (2011) 551.
[24] G.R. Desiraju, Acc. Chem. Res. 35 (2002) 565.
[25] Y.Y. Shao, J. Wang, M. Engelhard, C.M. Wang, Y.H. Lin, J. Mater. Chem. 20 (2010) 743.
[26] Y.C. Zhao, X.L. Yang, J.N. Tian, F.Y. Wang, L. Zhan, Int. J. Hydrogen Energy 35 (2010) 3249.
[27] M.M. Liu, Y.Z. Lu, W. Chen, Adv. Funct. Mater. 23 (2013) 1289.
[28] M.X. Chen, C.C. Zhang, X.C. Li, L. Zhang, Y.L. Ma, L. Zhang, X.Y. Xu, F.L. Xia, W. Wang, J.P. Gao, J. Mater. Chem. A 1 (2013) 2869.
[29] C.C. Chien, K.T. Jeng, Mater. Chem. Phys. 99 (2006) 80.
[30] J.F. Huang, S. Vongehr, S.C. Tang, H. Lu, X.K. Meng, J. Phys. Chem. C 35 (2010) 15005.
[31] D. Bera, S.C. Kuiry, M. McCutchen, A. Kruize, H. Heinrich, M. Meyyappan, S. Seal, Chem. Phys. Lett. 386 (2004) 364.
[32] H.C. Choi, M. Shim, S. Bangsaruntip, H.J. Dai, J. Am. Chem. Soc. 124 (2002) 9058.
[33] Y.J. Hu, P. Wu, Y.J. Yin, H. Zhang, C.X. Cai, Appl. Catal. B Environ. 112 (2012) 208.
[34] Y.C. Zhao, L. Zhan, J.N. Tian, S.L. Nie, Z. Ning, Electrochim. Acta 56 (2011) 1967.
[35] Y.C. Zhao, L. Zhan, J.N. Tian, S.L. Nie, Z. Ning, Int. J. Hydrogen Energy 35 (2010) 10522.
[36] Y.J. Hu, H. Zhang, P. Wu, H. Zhang, B. Zhou, C.X. Cai, Phys. Chem. Chem. Phys. 13 (2011) 4083.
[37] Z.L. Liu, B. Zhao, C.L. Gao, Y.J. Sun, Y. Shi, H.B. Yang, Z. Li, J. Colloid Interface Sci. 351 (2010) 233.
[38] Y. Mu, H. Liang, J. Hu, L. Jiang, L. Wan, J. Phys. Chem. B 109 (2005) 22212.
[39] S.F. Zheng, J.S. Hu, L.S. Zhong, L.J. Wan, W.G. Song, J. Phys. Chem. C 111 (2007) 11174.
[40] Z.P. Sun, X.G. Zhang, Y.Y. Liang, H.L. Li, Electrochem. Commun. 11 (2009) 557.